Ultramicroscopy 262 (2024) 113982

Contents lists available at ScienceDirect

Ultramicroscopy

journal homepage: www.elsevier.com/locate/ultramic

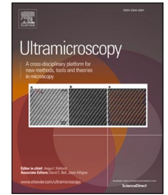

Standardization and quantification of backscattered electron imaging in scanning electron microscopy

Shih-Ming Wang [a,b], Yu-Cheng Chiu [a,b], Yu-Hsin Wu [a,b], Bo-Yi Chen [a], I-Ling Chang [b], Chih-Wei Chang [a,c,*]

[a] *Center for Condensed Matter Sciences, National Taiwan University, Taipei 10617, Taiwan*
[b] *Department of Mechanical Engineering, National Cheng Kung University, Tainan 70101, Taiwan*
[c] *Center of Atomic Initiative for New Materials (AI-MAT), National Taiwan University, Taipei 10617, Taiwan*

ARTICLE INFO

Keywords:
Backscattered electron
Thermal absorbance
Standardization
Electron microscopy

ABSTRACT

Backscattered electron (BSE) imaging based on scanning electron microscopy (SEM) has been widely used in scientific and industrial disciplines. However, achieving consistent standards and precise quantification in BSE images has proven to be a long-standing challenge. Previous methods incorporating dedicated calibration processes and Monte Carlo simulations have still posed practical limitations for widespread adoption. Here we introduce a bolometer platform that directly measures the absorbed thermal energy of the sample and demonstrates that it can help to analyze the atomic number (Z) of the investigated samples. The technique, named Atomic Number Electron Microscopy (ZEM), employs the conservation of energy as the foundation of standardization and can serve as a nearly ideal BSE detector. Our approach combines the strengths of both BSE and ZEM detectors, simplifying quantitative analysis for samples of various shapes and sizes. The complementary relation between the ZEM and BSE signals also makes the detection of light elements or compounds more accessible than existing microanalysis techniques.

1. Introduction

The conservation of energy and charge impose that any system should obey $A = 1\text{-}R\text{-}T$ (where A is the absorbance, R is the reflectance, and T is the transmittance of the system). Thus when operating a scanning electron microscope (SEM) under $T = 0$ condition, $A = 1\text{-}R$ will be satisfied; that is, A is complementary to R. Because R is known to be sensitive to the average atomic number (Z) and thickness of the sample [1,2], the result provides the foundation for utilizing either R or A measurements in quantitative SEM analysis. SEM's exceptional capabilities in enabling material analysis with nanoscale resolution have firmly established it as an indispensable tool across diverse scientific and industrial domains.

In SEM, the measurement of R is carried out by a backscattered electrons (BSE) detector. Unlike ordinary SEM images acquired using secondary electrons (SE) that could only provide information for samples' surface topography and morphology, BSE imaging has gained prominence for its potential capability to conduct quantitative analysis based on image contrast. Compared to tools of electron probe microanalysis (EPMA) [3,4], BSE detectors also have the advantages of faster scanning speeds and more cost-effective pricing [5].

However, quantitative analysis of BSE images remains limited in practice. The primary challenge lies in that BSE detectors usually have little energy resolution and a limited solid angle, while BSEs generally cover broad energy distributions with wide take-off angles (measured from the specimen surface). As shown in Fig. 1(a), BSEs can be divided into two components, i.e. $R = R_{\text{high}} + R_{\text{low}}$, where R_{high} and R_{low} are the reflectance of electrons at high ($> 45^\circ$) and low take-off ($< 45^\circ$) angles, respectively. It is known that R_{high} contains primarily low-loss BSEs that can provide information on Z of the sample, while R_{low} provides channeling contrast, topographic variations, and multiple scatterings induced by dislocations or defects and it becomes dominant at low voltage [6–8]. Unfortunately, BSE detectors, often installed at high take-off angles, fail to detect R_{low}, which constitutes a substantial source of error in offering accurate Z analysis based on BSE imaging.

Moreover, SEMs produced by different manufacturers or distinct models come with their specific specifications and characteristics. The variations in instrumental design and settings can result in disparities in

* Corresponding author at: Center for Condensed Matter Sciences, National Taiwan University, Taipei 10617, Taiwan.
E-mail address: cwchang137@ntu.edu.tw (C.-W. Chang).

https://doi.org/10.1016/j.ultramic.2024.113982
Received 10 October 2023; Received in revised form 8 April 2024; Accepted 25 April 2024
Available online 26 April 2024
0304-3991/© 2024 Elsevier B.V. All rights reserved.

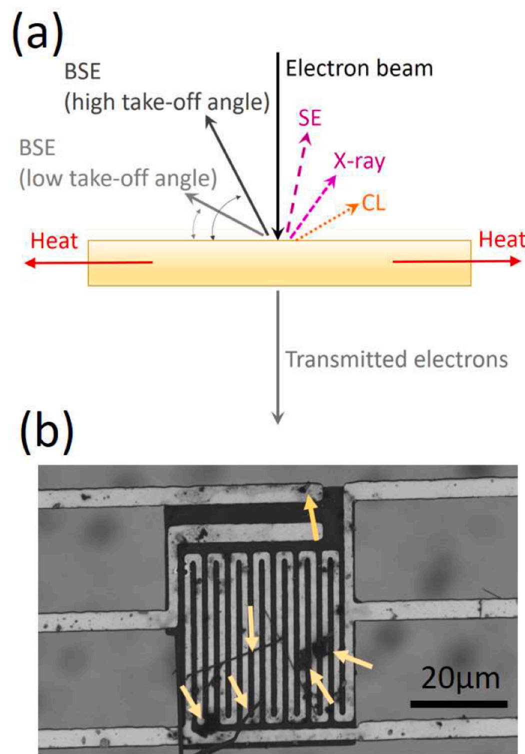

Fig. 1. (a) Schematic illustration of various detection methods in SEM. In general, any system should obey $A = 1\text{-}R\text{-}T$, where R includes BSEs at high ($> 45^\circ$) and low ($< 45^\circ$) take-off angles, T is the transmitted electrons, and A contains secondary electrons (SE), cathodoluminescence (CL), X-rays, heat (A_{th}), etc. (b) SEM image of a bolometer platform that enables direct A_{th} measurement on samples deposited on it (denoted by the arrows).

image acquisition, complicating the standardization process across diverse SEMs. Additionally, users often make arbitrary adjustments to operation conditions such as image brightness and contrast, leading to complex variations in the grayscale of BSE images. Furthermore, since BSE signals can be influenced by the incident angle of the electron beam, it is imperative for standard samples to be meticulously polished and devoid of nanoscale inhomogeneity. In essence, the accurate quantification of BSE signals relies on maintaining R_{high}/R_{low} to be a robust constant immune from the above perturbations. However, R_{high}/R_{low} can be easily perturbed in practical scenarios. This lack of a streamlined standardization procedure has inclined researchers to showcase SEM images primarily for aesthetic purposes rather than as conveyors of quantifiable and reproducible scientific information.

Many efforts have been devoted to overcoming the difficulty. A voltage bias applied on the sample stage can increase R_{high}/R_{low} and mitigate uncertainties arising from R_{low}. An energy-selective BSE detector can be employed to remove unwanted SE and high-loss BSE signals [9]. Quantitative analysis of BSE images can be carried out by comparing BSE signals with results from Monte-Carlo simulations or samples of known structures so that R_{high}/R_{low} can be recalibrated in the presence of perturbations [10–13]. Fundamentally, it is essential to recognize that factors such as R_{low}, secondary electrons (SEs), charging effects, and electron beam absorbed currents can exhibit considerable variations. They render the electronic readouts of BSE, primarily based on R_{high} detection, inadequate as a foundational standardization basis, thereby posing a formidable challenge in establishing a correlation between BSE detection and the sample's Z. In this paper, we introduce a standardization procedure rooted in the conservation of energy, offering the capacity to reproduce and transfer results consistently across diverse SEMs.

Although A contains various forms, including SEs, electron beam absorbed currents, cathodoluminescence, X-rays, heat, etc., we have recently introduced a bolometer platform integrated with an SEM that allows direct measurements of samples' thermal absorbance (A_{th}) under electron beam irradiation [14]. The detection schemes of BSE and A_{th} are shown in Fig. 1(a). The bolometer platform is supported by suspended SiN_x beams with Pt film thermometers (whose temperature coefficient of resistance is 0.1~0.15 %/K) deposited on it [15–17], as displayed in Fig. 1(b). This integrated platform is affixed to a piezo-driven XY-scanner, facilitating raster scans for A_{th} mapping of the investigated samples. Unlike BSE detectors that can only collect a portion of R, here all the absorbed heat can be collected by the bolometer. The total incident power is achievable by multiplying the provided V_{acc} and the current detected by a Faraday cup. Thus, A_{th} can be experimentally determined and we have demonstrated that most of A is converted into heat, i.e., $A_{th}/A = 98$ % [14,18]. Based on the complementary relation $R = 1\text{-}A$, we can regard $1\text{-}A_{th}$ as a nearly ideal BSE detector, similar to the role of integrating spheres in optic measurements [19]. The bolometer platform serves as the foundation for precise Z analysis through SEM, leading us to name this technique "Atomic Number Electron Microscopy" (ZEM).

When operating an SEM to image a sample with finite thickness, there exists a threshold V_{acc} (also known as the most efficient electron beam heating voltage [18], V_{MEEHV}) under which $T = 0$ can be satisfied. As shown in Fig. 2(a), A is nearly independent of V_{acc} when $V_{acc} < V_{MEEHV}$, which makes the condition suitable for quantification of SEM images. On the other hand, A monotonically decreases for $V_{acc} > V_{MEEHV}$. For the case of $T > 0$, the complementary relation $A = 1\text{-}R$ no longer holds and additional calibration would be needed to calibrate A.

Compared with BSE imaging, the ZEM has several unique features. Firstly, while BSE detectors often struggle to detect low-Z materials due to their weaker scattering power, ZEM exhibits remarkable sensitivity to light elements and compounds. Secondly, the limited collection angle and vacuum chamber space only allow R_{high} to be measured, making the intensity of BSE signals a relative quantity. In contrast, because all the absorbed heat is collected by the bolometer, A_{th} is an absolute quantity, which would facilitate the implementation of a standardization procedure discussed later. Thirdly, unlike the arbitrary brightness and contrast adjusted by users in BSE imaging, no such adjustments are allowed in ZEM, ensuring the reproducibility of ZEM images across various laboratories and users. Fourthly, ZEM images are noted for their highly accurate quantification, characterized by a mere ~2 % systematic error stemming from other non-thermal excitations mentioned above. Finally, unlike BSE detectors, which may have biased grids or thin protection layers to filter low-energy electrons, ZEM imaging operates without such filters. The inclusion of energy filters in BSE detectors can introduce complexities into the quantification of BSE signals [9], while the signal interpretation in ZEM remains straightforward.

Fig. 2(b) summarizes ZEM and BSE signals vs. Z. ZEM signals for the elements under investigation have been normalized to those of SiN_x, whose A_{th} is calibrated by measuring the total electron beam energy and absorbed thermal energy, yielding $A_{th}(SiN_x) = 0.89$ [14]. The calibration procedure gives good agreements with Monte Carlo simulation using the CASINO program [20–22]. In principle, a similar calibration procedure can be carried out in BSE images if standard samples are provided. However, various factors could affect the BSE detection and make the quantitative analysis difficult in practice. We have examined the grayscale values of BSE images from the same samples investigated with ZEM and applied analogous calibration procedures. Nevertheless, the BSE images exhibit significant deviations from the simulated curve, a phenomenon that has also been noted by A. Garitagoitia Cid et al. [23].

Yet ZEM has its own constraints. Firstly, in comparison to BSE electronics, our current bolometer exhibits a considerably slower thermal response, resulting in time-consuming ZEM acquisition for larger sample areas. Secondly, a meticulous sample preparation process is requisite for depositing samples onto the suspended bolometer platform, prohibiting the acquisition of ZEM images for thin films on substrates or

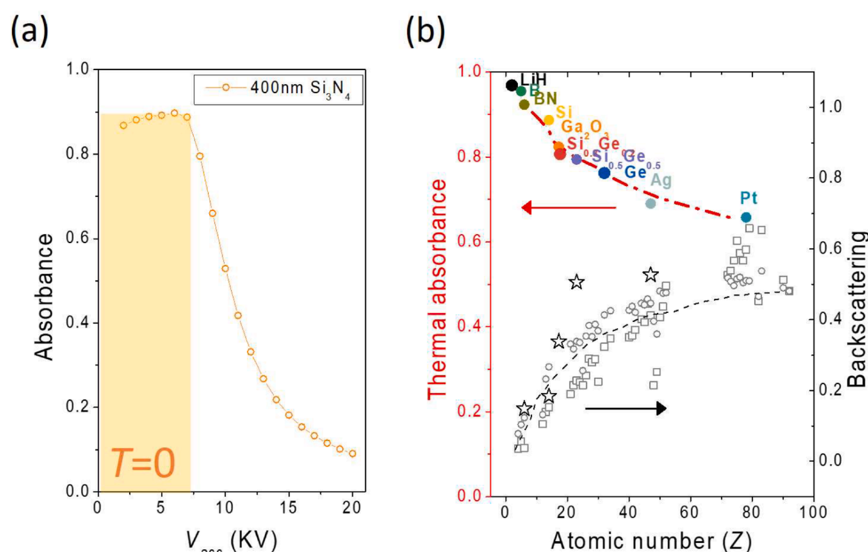

Fig. 2. (a) Simulated A vs. V_{acc} for a 400 nm thick SiN_x film. For $V_{acc} < 8$ KV, the electrons cannot penetrate the SiN_x film. When $T = 0$ condition (denoted shaded area) is satisfied, A is nearly independent of V_{acc}. (b) A_{th} & BSE vs. Z. The experimental data of A_{th} (solid color symbols, from our earlier work [14]) and BSE. The data from Refs. [14,23] are displayed as open black stars and open gray symbols, respectively. The results of CASINO simulation for A_{th} (red dash-dotted curve) and BSE (dashed curve) under a $V_{acc} = 5$ KV electron beam are also shown for comparison. The BSE signals from Refs. [14,23] are normalized to that of the simulated result at $Z = 10$ and 92, respectively.

heavy specimens. To address these limitations, we have devised a standardization scheme that allows BSE to harness the advantages of ZEM in providing precise and quantitative data, while ZEM can benefit from BSE's rapid electronic response and straightforward sample preparation methods.

2. Methodology

We design the standardization procedure based on the fact that our ZEM setups are not commonly available but BSE detectors are usually installed in many SEMs. Specifically, we correlate the signals of ZEM and BSE using:

$$A_{th} = f(I_{BSE}, \ldots) \quad (1)$$

where A_{th} is an absolute physical quantity, acquired through ZEM's aforementioned measurements. I_{BSE} is BSE's electronic signals, influenced by instrumental configurations and user adjustments, and f would be a function of various factors mentioned above, as denoted by "…" in Eq. (1). Given $A_{th}/A = 98$ %, 1-A_{th} can be considered a nearly ideal BSE detector, akin to the function of an integrating sphere in optics that collects R from all angles. Consequently, the ZEM image can serve as the standard image.

Fig. 3 illustrates the workflow of the standardization procedure. (1) A ZEM user supplies a standard sample (Fig. 3(a)), which is then placed on the bolometer, and wire-bonded on a chip carrier to capture an original A_{th} image (Fig. 3(b)). The brightness of A_{th} represents the absolute value of thermal absorbance. It is colorized by converting the 256 grayscale into RGB values based on Fig. 3(c). (2) Subsequently, the standard sample on the bolometer and the original A_{th} image is transferred to an SEM user, as depicted in Fig. 3(d & e). The SEM user acquires a BSE image of the standard sample, as shown in Fig. 3(f). By employing a computer program discussed later, a function f that correlates the intensities of the BSE image and the original A_{th} image can be obtained, as shown in Fig. 3(g). (3) The SEM user employs the same f for standardizing other BSE images once all the settings of the SEM are kept unchanged, as illustrated in Fig. 3(h & i). These standardized BSE images are referred to as "converted A_{th} images". In case of any setting adjustments, the SEM user can repeat step (2) to recalibrate the BSE images and find a new f. Similar procedures can be extended to other users or SEMs to generate additional converted A_{th} images. Of course, these converted A_{th} images and the samples can be sent to the ZEM user to double-check the accuracy of the converted A_{th}'s. Because all the converted A_{th} images provide the absolute value of thermal absorbance, they would make quantitative analysis of BSE images possible.

We now discuss more details based on the Monte Carlo simulations using the CASINO program (Version 3.3.0.4) [20–22]. The MONSEL Defaults physical model was used for the simulation. A simulation window was specifically configured within the model to replicate the characteristics of a BSE detector, positioned at a take-off angle of 50° and encompassing a collection angle of 80°. We typically introduced a total of 100,000 electrons into the system to get A and I_{BSE}. To get ZEM and BSE images, A and I_{BSE} mapping of various elements with $Z = 6{\sim}82$ on a Si_3N_4 substrate are respectively obtained by the CASINO scanning function under $V_{acc} = 5$ KV, as respectively shown in Fig. 3(b). Note that the effective Z=$(xZ_A+yZ_B)/(x + y)$ for a binary compound A_xB_y (where the atomic numbers are respectively Z_A and Z_B for A and B). The image of ZEM is colorized by converting the grayscale of A into RGB values based on Fig. 3(c). From Fig. 3(g), we note that A is an absolute value, which varies from 0.61 to 0.93. In contrast, I_{BSE} exhibits a broader span, covering values from 0 to 1, attributable to image contrast enhancement.

To find f, we have developed a computer program that first equalizes the pixel numbers of images and then compares, pixels by pixels, the brightness of A and I_{BSE}. As shown in Fig. 3(g), here a linear function $A = -0.35I_{BSE} + 0.95$ would suffice as a good fit. Although the errors of f and x are given by the Monte Carlo simulation, the complementary relation between A and I_{BSE} makes the signal-to-noise ratio (S/N) of A 34 times higher than that of I_{BSE} for light elements. Thus, the S/N in the converted A_{th} image will be improved when investigating light elements or compounds. After obtaining the f, the SEM user can employ the same f to standardize other BSE images. As shown in Fig. 2(a), A would be nearly independent of V_{acc} once $T = 0$ is satisfied. Thus the standardization procedure would be applicable even if the ZEM and the BSE images are taken at different V_{acc}'s.

3. Results

Having justified our approach, now we check whether the

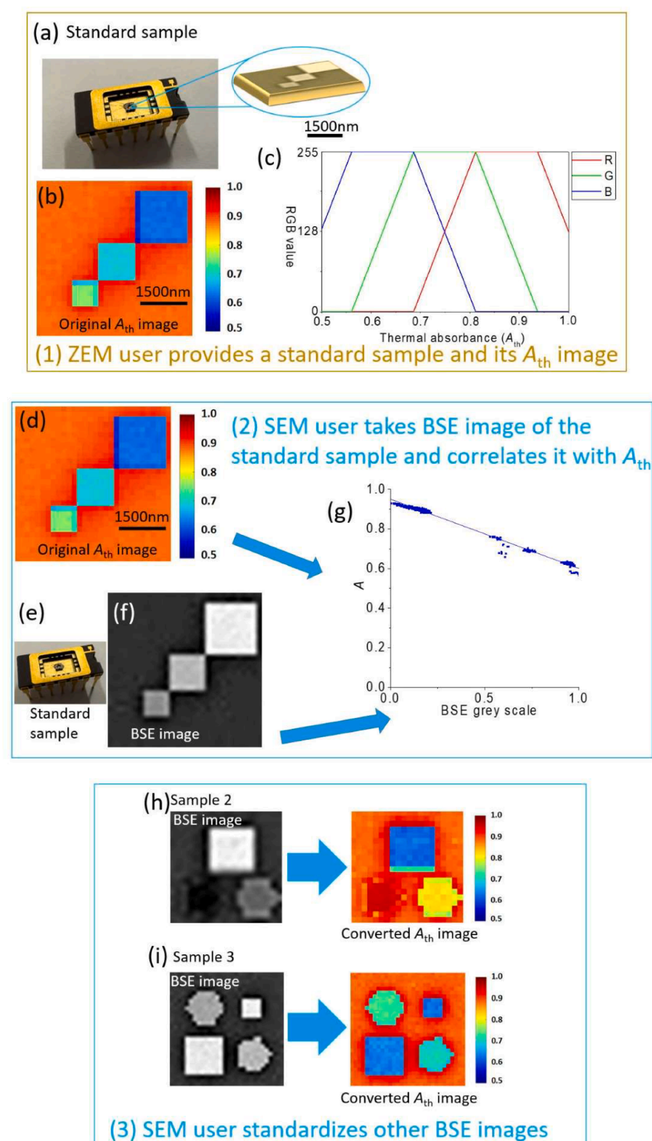

Fig. 3. The workflow of the standardization procedure. Here the original A_{th} images and BSE images are obtained from the CASINO simulation. (a) A standard sample consisting of Ge ($Z = 32$), In ($Z = 49$), and Pb ($Z = 82$) on a Si_3N_4 ($Z = 10$) is provided by a ZEM user, who deposits it on the bolometer mounted on a chip carrier. (b) The ZEM user employs ZEM to obtain an original A_{th} image, which is colorized by converting the grayscale into RGB based on (c). (d & e) The original A_{th} image and the standard sample are transferred to a SEM user, who then takes a BSE image of the standard sample, as shown in (f). (g) A computer program correlates the intensities of the original A_{th} image and the BSE image to obtain a function *f*. (h & i) The SEM user can employ the same *f* for standardizing other BSE images once all the settings of the SEM are kept unchanged. Because the absolute color bar can be provided for all the converted A_{th} images, they would make the standardization of BSE images possible.

standardization procedure could work for realistic cases. As shown in Fig. 4(a), a ZEM image of SiC nanoparticles and nanowires (purchased from Novarials, Catalog Number: NovaWire-SiC-100-RD) deposited on our bolometers taken under $V_{acc} = 5$ KV by a Zeiss Auriga SEM is selected as the standard sample. The corresponding BSE images under different V_{acc}'s are taken by an annular BSE detector using JEOL JSM-7800F Prime SEM, as shown in Fig. 4(b). We find that a BSE image obtained using $V_{acc} = 6$ KV with 2 KV stage bias (denoted as $V_{acc} = 6$–2 KV, which corresponds to a landing voltage 4 KV) gives the clearest sample features and thus the image is chosen as a representative image. As shown in Fig. 4(c), we find that A_{th} varies from 0.71 to 0.95, representing the absolute value of thermal absorbance. On the other hand, I_{BSE} spans a wider range, covering from 0.15 to 0.52 due to image contrast enhancement adjusted by the user. The data are fitted using $A_{th} = -0.52 I_{BSE} + 0.99$. For light elements, the S/N of A_{th} is 3.6 times higher than that of I_{BSE}. The converted A_{th} is shown in Fig. 4(d). Because A_{th} would reduce at tilted facets and edges, the brightest A_{th} is used for analyzing the *Z* of a sample [14]. The *Z* of the SiC nanowire read out from the converted A_{th} image is 6.6~12.7, consistent with the expected $Z = 10$ from the SiC.

We can take advantage of the BSE detector's fast electronic responses to obtain large-area BSE images of SiC nanowires at other regions as well as SnS micrograins located at another device under $V_{acc} = 4$ KV and 6–2 KV, respectively. Fig. 4(e) shows a representative large-area BSE image at $V_{acc} = 6$–2 KV of a bolometer platform with SiC nanowires deposited on it. Because the brightness, contrast, and working distance are kept the same, we use the same *f* to obtain their converted A_{th} images, as shown in Fig. 4(f). Adjacent to the suspended bolometer platform, there are vacuum regions where the incident electrons are all transmitted. For these $T \sim 1$ regions, the criteria for the standardization procedure are not obeyed and thus the converted A_{th} gives incorrect colors, as denoted in Fig. 4(f).

We have conducted additional scans of the samples using ZEM to validate the quantitative accuracy of the converted A_{th} images, as depicted in Fig. 5. It is worth noting that the resolution of the converted A_{th} images may be compromised, as they are extracted from low-resolution, large-area BSE images. From Fig. 5, we find $Z = 7.7 \sim 10.2$ for SiC ($Z = 10$), and $Z = 27.2 \sim 31.7$ for SnS ($Z = 33$). Compared with the large uncertainties given by the BSE shown in Fig. 2(b), the result demonstrates that our standardization procedure improves the determination of *Z* for the investigated samples.

We have repeated the process for different samples and the results are summarized in Fig. 6. We find that the standardization procedure generally gives good agreements with the result of the original A_{th} and the CASINO simulation. But we also notice strong deviations from a Ge micrograin and an Ag nanowire, whose A_{th}'s are much higher than expected. One possible explanation is that R_{low} is more prominent in these two samples and escape detection by the BSE detector, leading to a reduced BSE signal and, consequently, the larger converted A_{th} seen in Fig. 6. This increase of R_{low} for these specific samples may be attributed to either an intrinsic property associated with higher *Z* samples or the presence of uneven sample surfaces, which might hinder the detection of their BSEs by the BSE detector. To reduce these perturbations, it is suggested to analyze flat regions of a sample that are free from topographical variations to accurately obtain its *Z*.

We now discuss the cases when BSE images are taken at V_{acc}'s significantly different from those used in acquiring A_{th}. As shown in Fig. 2(a), although the simulation suggests A_{th} to be nearly independent of V_{acc} once $V_{acc} < V_{MEEHV}$ is satisfied, operating SEM under low V_{acc} is known to reduce the interacting volume of the electron beam to the sample, rendering the BSE signals to be more sensitive to surface morphology. Indeed, the BSE image of a SiC nanoparticle under $V_{acc} =$ 2KV shows carbon contamination at the surface, which is unseen in the original A_{th} image taken under $V_{acc} =$ 5KV. Consequently, the I_{BSE} vs. A_{th} is distributed like a L-shape pattern and a nonlinear *f* is needed to give a good fit, as shown in Fig. 7(a). The presence of carbon contamination leads to the converted A_{th} image displayed in Fig. 7(b) a reddish tint corresponding to $Z = 6.73$, which is expected for a thin carbon layer deposited on SiN_x.

So far the above discussions are based on the $T = 0$ condition and the complementary relation $A = 1$-R is held. If $T > 0$, *A* would be V_{acc}-dependent, rendering it less suitable as a standard quantity. One might wish to correlate $A_{th}(V_{acc} > V_{MEEHV})$ with $A_{th}(V_{acc} < V_{MEEHV})$ to enable the standardization procedure. However, transmitted electrons would play a role similar to that of R_{low} in BSE detection, meaning that a portion of electrons escapes detection by our bolometer. Thus, making the ratio $A_{th}(V_{acc} < V_{MEEHV})/A_{th}(V_{acc} > V_{MEEHV})$ immune from other

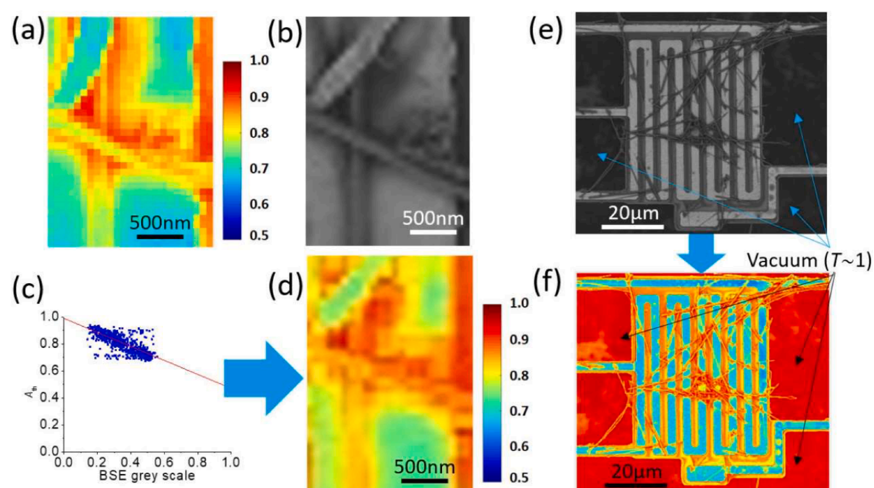

Fig. 4. Experimental demonstration of the standardization procedure. (a) An original A_{th} image of SiC nanowires deposited on a bolometer which serve as the standard sample. (b) The corresponding BSE image. (c) Brightness distribution of the original A_{th} image vs the BSE image. Here we obtain $A_{th} = -0.52I_{BSE} + 0.99$. (d) The f is used for converting the BSE image shown in (b) into a converted A_{th} image. (e & f) The same f is used for standardizing a large-area BSE image taken under $V_{acc} = 6$–2 KV into a converted A_{th} image. Note that because of the near-unity electron transmission ($T \sim 1$) in the denoted vacuum regions, the corresponding red color in the converted A_{th} image is incorrect.

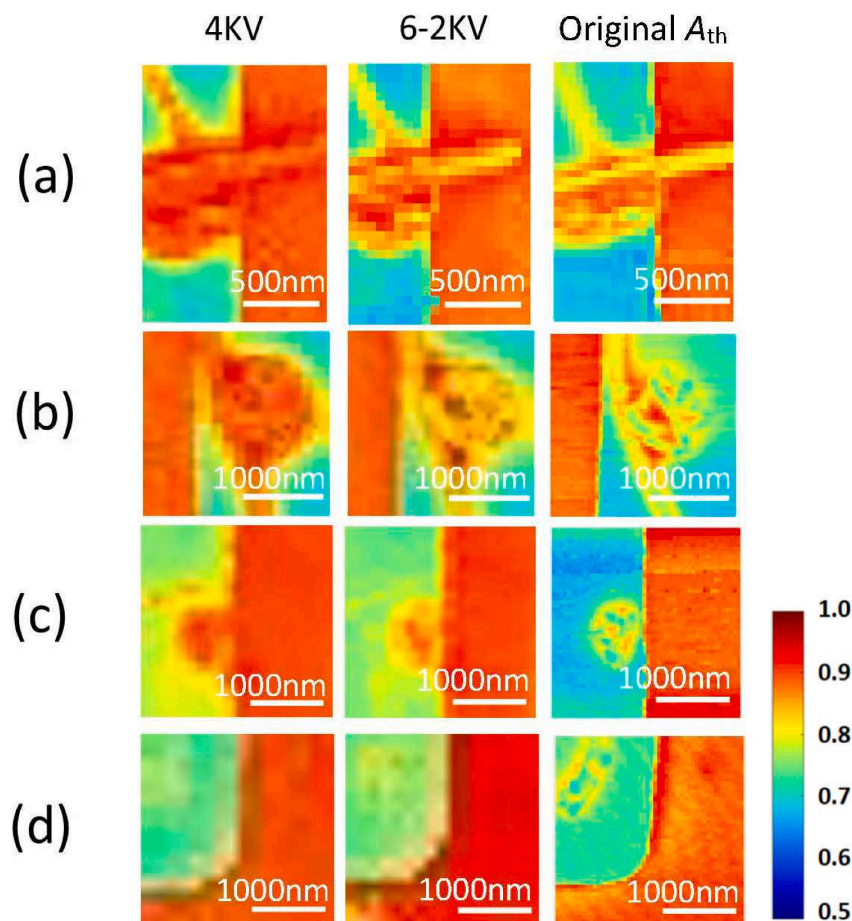

Fig. 5. Selected regions of the converted A_{th} images taken under $V_{acc} = 4$ KV and 6–2 KV, showing (a & b) a SiC nanoparticle and a nanowire, (c) a SiC nanoparticle, and (d) a SnS micrograin. The corresponding original A_{th} images taken under $V_{acc} = 5$ KV are shown for comparison.

perturbations would become as intricate as previous BSE calibration schemes. To demonstrate it, Fig. 7(c) shows the correlation between $A_{th}(V_{acc} = 5\text{ KV})$ and $A_{th}(V_{acc} = 15\text{ KV})$ (here $V_{MEEHV} = 7.6$ KV). The same sample shown in Fig. 4(f) is used, but it is now converted from BSE image taken under $V_{acc} = 15$ KV. As shown in Fig. 7(d), a lot of samples on the surface become invisible due to large electron penetration depth at $V_{acc} = 15$ KV. Yet, as explained above, the Z's of the SiC nanowires read out from the converted A_{th} image appears incorrect; $Z = 4.2 \sim 6.8$,

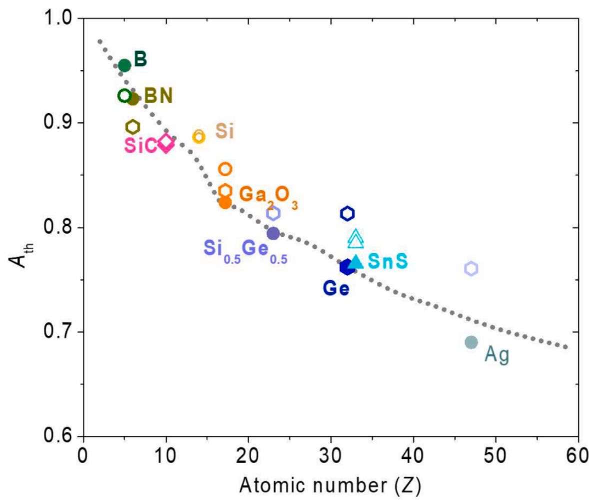

Fig. 6. Summary for A_{th} vs. Z of the investigated samples based on original A_{th} images (solid symbols) and converted A_{th} images (open symbols). Materials of the same kind are plotted using identical colors. The dotted curve is the result based on CASINO simulation.

14.8 ~ 15.5, 37 ~ 38.1 for SiC nanowires suspended in vacuum, on SiN_x, on Pt film, respectively. Therefore, it is recommended to maintain the $T = 0$ condition for conducting the standardization procedure.

Based on the above discussions, we summarize the workflow of the standardization procedure in Fig. 8. It should be emphasized that when the imaging conditions (such as working distance, tilt angles, brightness, or contrast) of the SEM user's change, the procedure repeating Fig. 3(f) will be needed to acquire a new function f. But if the SEM user's V_{acc} changes, the ZEM user will need to provide a new A_{th} image using an identical V_{acc}. Therefore, the accuracy of the converted A_{th} images presented above is significantly influenced by the quality of the original A_{th} images. Ensuring the quality of the ZEM acquisition is of paramount importance for SEM users. Although ZEM acquisition may be time-consuming, high quality original A_{th} images can be obtained if the ZEM apparatus is kept at a stable, drift-free, low-noise environment. In this context, the ZEM user functions similarly to centralized agencies that oversee standards like kilogram or time, providing standard samples and images for calibration to other SEM users. Because BSE image calibration has never established a similar process, ZEM creates an innovative advancement in this domain.

Lastly, we note that the complementary relation between A and R may be applied to scanning transmission electron microscopy (STEM). Because of STEM's high V_{acc}, we instead have $R \sim 0$ and A is

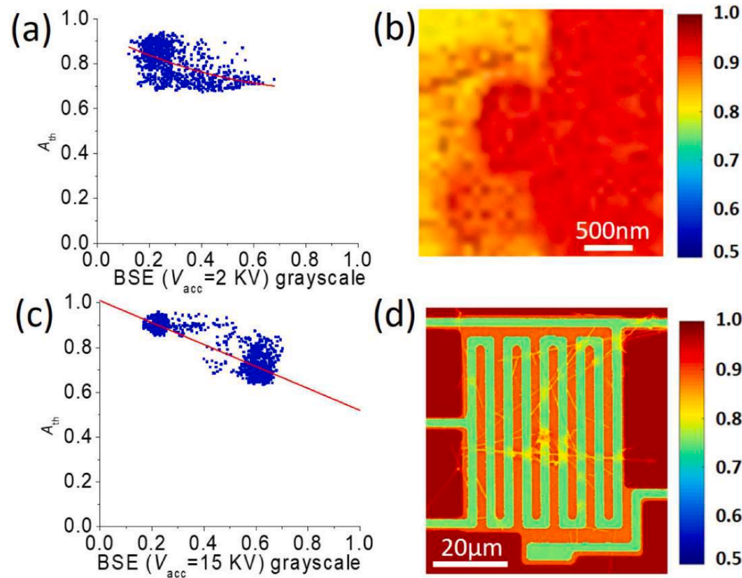

Fig. 7. Testing the standardization procedure for BSE images taken under $V_{acc} = 2$ KV and $V_{acc} = 15$ KV. (a) Brightness distribution of the original A_{th} image taken under $V_{acc} = 5$ KV vs. the BSE image taken under $V_{acc} = 2$ KV. A nonlinear function $A_{th} = 0.31\, I_{BSE}^2 - 0.62 I_{BSE} + 0.94$ is employed to fit the data. (b) The converted A_{th} image. Here the SiC nanoparticle sample is identical to that shown in Fig. 5(c). (c) $A_{th}(V_{acc} = 5\text{ KV})$ vs. $I_{BSE}(V_{acc} = 15\text{ KV})$. Here we have $A_{th} = -0.49 I_{BSE} + 1.01$. (d) The corresponding converted A_{th} image. Here the sample is identical to that shown in Fig. 4(f).

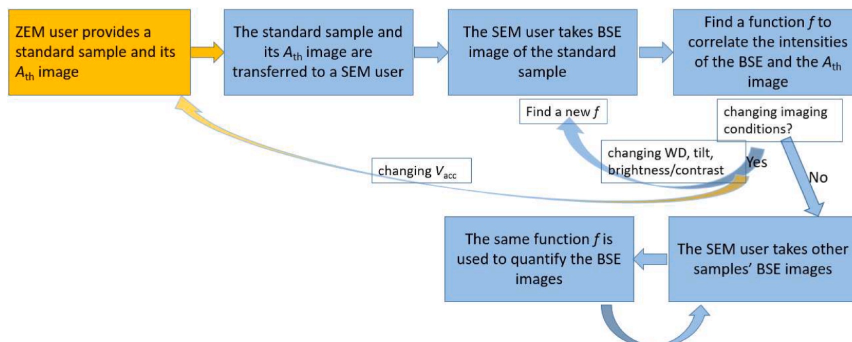

Fig. 8. Summary of the workflow for the standardization and quantification of BSE images.

complementary to T. The Z analysis in STEM is carried out by high-angle annular dark-field (HAADF) imaging, in which a $Z^{1.7}$-dependent scattering angle contributes to the image contrast. However, similar to BSE's limitations, HAADF images would have difficulty detecting light elements and compounds. The proposed standardization procedure remains applicable to STEM when A_{th} constitutes a substantial portion of A.

In conclusion, we present a method to standardize BSE imaging using ZEM, which excels in detecting light elements and compounds. This standardization process combines the advantages of ZEM and BSE, delivering a robust and consistent protocol adaptable to diverse SEM setups and user needs. The workflow offers an efficient means of conducting quantitative BSE image analysis, improving the accuracy of Z analysis using SEM. The standardization procedure surpasses previous constraints in detecting low Z materials, ensuring SEM a pivotal tool for scientists and engineers across diverse disciplines.

Declaration of generative AI in scientific writing

During the preparation of this work the authors used ChatGPT in order to improve English writing. After using this tool/service, the authors reviewed and edited the content as needed and take full responsibility for the content of the publication.

CRediT authorship contribution statement

Shih-Ming Wang: Data curation, Formal analysis, Investigation. **Yu-Cheng Chiu:** Data curation, Formal analysis, Investigation. **Yu-Hsin Wu:** Data curation, Formal analysis, Investigation. **Bo-Yi Chen:** Formal analysis, Investigation, Methodology. **I-Ling Chang:** Investigation, Resources, Supervision, Software. **Chih-Wei Chang:** Conceptualization, Data curation, Formal analysis, Funding acquisition, Investigation, Methodology, Project administration, Resources, Software, Supervision, Validation, Visualization, Writing – original draft, Writing – review & editing.

Declaration of competing interest

The authors declare that they have no known competing financial interests or personal relationships that could have appeared to influence the work reported in this paper.

Data availability

Data will be made available on request.

Acknowledgments

This work is supported by the Ministry of Science and Technology of Taiwan (MOST 111-2112-M-002-043-MY3 and 110-2119-M-002-010-MBK), and Center of Atomic Initiative for New Materials, National Taiwan University, from the Featured Areas Research Center Program within the framework of the Higher Education Sprout Project by the Ministry of Education in Taiwan (108L9008).

References

[1] H. Niedrig, Principles of Electron Backscattering on Solids, Mikroskopie 34 (1978) 167.
[2] H. Niedrig, Film-Thickness Determination in Electron-Microscopy - Electron Backscattering Method, Opt. Acta 24 (1977) 679.
[3] R. Rinaldi, X. Llovet, Electron Probe Microanalysis: A Review of the Past, Present, and Future, Microsc. Microanal. 21 (2015) 1053.
[4] X. Llovet, A. Moy, P.T. Pinard, J.H. Fournelle, Electron probe microanalysis: A review of recent developments and applications in materials science and engineering, Prog. Mater. Sci. 116 (2021) 100673.
[5] S.I. Wright, M.M. Nowell, R. de Kloe, P. Camus, T. Rampton, Electron imaging with an EBSD detector, Ultramicroscopy 148 (2015) 132.
[6] T. Aoyama, M. Nagoshi, H. Nagano, K. Sato, S. Tachibana, Selective Backscattered Electron Imaging of Material and Channeling Contrast in Microstructures of Scale on Low Carbon Steel Controlled by Accelerating Voltage and Take-off Angle, ISIJ Int 51 (2011) 1487.
[7] T. Aoyama, M. Nagoshi, K. Sato, Quantitative analysis of angle-selective backscattering electron image of iron oxide and steel, Microscopy 64 (2015) 319.
[8] K. Sato, H. Sueyoshi, K. Yamada, Characterization of complex phase steel using backscattered electron images with controlled collection angles, Microscopy 64 (2015) 297.
[9] A.G. Cid, M. Sedighi, M. Loffler, W.F. van Dorp, E. Zschech, Energy-Filtered Backscattered Imaging Using Low-Voltage Scanning Electron Microscopy: Characterizing Blends of ZnPc-C-60 for Organic Solar Cells, Adv. Eng. Mater. 18 (2016) 913.
[10] E. Muller, D. Gerthsen, Composition quantification of electron-transparent samples by backscattered electron imaging in scanning electron microscopy, Ultramicroscopy 173 (2017) 71.
[11] M. Calkovsky, E. Muller, D. Gerthsen, Quantitative analysis of backscattered-electron contrast in scanning electron microscopy, J. Microsc. 289 (2023) 32.
[12] T. Kowoll, E. Muller, S. Fritsch-Decker, S. Hettler, H. Stromer, C. Weiss, D. Gerthsen, Contrast of Backscattered Electron SEM Images of Nanoparticles on Substrates with Complex Structure, Scanning (2017) (2017) 4907457.
[13] R. Skoupy, T. Fort, V. Krzyzanek, Nanoscale Estimation of Coating Thickness on Substrates via Standardless BSE Detector Calibration, Nanomaterials 10 (2020) 332.
[14] C.C. Lin, S.M. Wang, B.Y. Chen, C.H. Chi, I.L. Chang, C.W. Chang, Scanning Electron Thermal Absorbance Microscopy for Light Element Detection and Atomic Number Analysis, Nano Lett 22 (2022) 2667.
[15] M.C. Wingert, Z.C.Y. Chen, S. Kwon, J. Xiang, R.K. Chen, Ultra-sensitive thermal conductance measurement of one-dimensional nanostructures enhanced by differential bridge, Rev. Sci. Instrum. 83 (2012) 024901.
[16] T.K. Hsiao, H.K. Chang, S.C. Liou, M.W. Chu, S.C. Lee, C.W. Chang, Observation of room temperature ballistic thermal conduction persisting over 8.3 micrometers in SiGe nanowires, Nat. Nanotechnol. 8 (2013) 534.
[17] T.K. Hsiao, B.W. Huang, H.K. Chang, S.C. Liou, M.W. Chu, S.C. Lee, C.W. Chang, Micron-scale ballistic thermal conduction and suppressed thermal conductivity in heterogeneously-interfaced nanowires, Phys. Rev. B 91 (2015) 035406.
[18] P.Y. Yuan, J.Y. Wu, D.F. Ogletree, J.J. Urban, C. Dames, Y.B. Ma, Adapting the Electron Beam from SEM as a Quantitative Heating Source for Nanoscale Thermal Metrology, Nano Lett 20 (2020) 3019.
[19] S.A. Mann, B. Sciacca, Y.Y. Zhang, J. Wang, E. Kontoleta, H.Y. Liu, E.C. Garnettt, Integrating Sphere Microscopy for Direct Absorption Measurements of Single Nanostructures, ACS Nano 11 (2017) 1412.
[20] P. Hovington, D. Drouin, R. Gauvin, CASINO: A new Monte Carlo code in C language for electron beam interaction .1. Description of the program, Scanning 19 (1997) 1.
[21] P. Hovington, D. Drouin, R. Gauvin, D.C. Joy, N. Evans, CASINO: A new Monte Carlo code in C language for electron beam interactions .3. Stopping power at low energies, Scanning 19 (1997) 29.
[22] D. Drouin, P. Hovington, R. Gauvin, CASINO: A new Monte Carlo code in C language for electron beam interactions .2. Tabulated values of the Mott cross section, Scanning 19 (1997) 20.
[23] A.G. Cid, R. Rosenkranz, M. Loffler, A. Clausner, Y. Standke, E. Zschech, Quantitative analysis of backscattered electron (BSE) contrast using low voltage scanning electron microscopy (LVSEM) and its application to $Al_{0.22}Ga_{0.78}N$/GaN layers, Ultramicroscopy 195 (2018) 47.